European Journal of Mathematics and Statistics
Vol 4 | Issue 4 | August 2023
ISSN 2736-5484

RESEARCH ARTICLE

Blood Flow Modeling in Constricted Arteries Under Body Acceleration and Wall Slip Using Two-Layered Bingham Plastic Fluid

Mokshed Ali*

ABSTRACT

Analysis is done on a two-layered Bingham Plastic model of restricted, thin arteries with periodic body acceleration. The model essentially consists of a centre layer with a core of suspended red blood cells and an outer layer with a peripheral plasma layer. It has been assumed that the rheology of blood in the core region has been classified as a Newtonian fluid with the PPL and a non-Newtonian fluid obeying the law of Bingham plastic model. This model has been used to investigate how blood flow in stenotic arteries is affected by body acceleration, the non-Newtonian character of blood, and a velocity slip at the wall. Analytical equations for axial velocity, flow rate, wall shear stress, and apparent viscosity are produced by using the perturbation method, and their variations with respect to various parameters are shown in the figures and explained in this article. Due to a wall slip, it is seen that while velocity and flow rate rise, effective viscosity falls. The impact of body acceleration significantly increases flow rates and speed. The physiological effects of this theoretical modelling for blood flow conditions are also briefly looked at.

Keywords: Bingham plastic, body acceleration, flow resistance, shear stress.

Submitted: March 20, 2023

Published: August 31, 2023

10.24018/ejmath.2023.4.4.223

Department of Mathematics, Barkhetri College Mukalmua, India.

Corresponding Author:
e-mail: mokshed.ali7@gmail.com

1. Introduction

The majority of fatal cases are known to be caused by circulatory diseases, and stenosis or arterioscleriosis is one such worrying instance [1], [2]. The term "stenosis" refers to an abnormal growth that narrows the diameter of an artery. It is one of the most common diseases and can cause major circulatory disorders by restricting or obstructing the blood flow to various body organs and tissues [3]. Recently, Ponalgusamy [4], Biswas and Chakraborty [5] have developed mathematical models for blood flow through stenosed arterial segment, by taking a velocity slip condition at the constricted wal considering blood as a Newtonian fluid. The existence of a core area of suspension containing nearly all the erythrocytes and a layer of cell-poor plasma (Newtonian fluid) for blood flowing through small arteries has been empirically demonstrated by [6], [7]. In a two-layered model of blood flow in tiny diameter tubes, [6] presupposed that the core and periphery fluids were Newtonian fluids with varying viscosities. Several researchers have noted that under specific flow conditions, blood has a finite yield stress [8], [9]. One intriguing and unique example of a material having yield stress is referred to as Bingham plastic, which exhibits a straight line consistency curve or flow behaviour [8], [9]. Until the yield stress is reached, this specific material deforms elastically. Nevertheless, after this stress is exceeded, it flows like a Newtonian fluid, with shear stress being linearly proportional to share rate of shear strain [10]. Hence, it appears plausible to think of blood acting as a Bingham plastic in the core region of a restricted artery.

As a muscular pump, the human heart creates a pressure difference between its systolic and diastolic states, commonly referred to as the pressure pulse, which doctors measure at the wrist. Pulsatile flow is the term used to describe the blood flow caused by this pressure pulse [11], [12]. The human body may also experience accelerations in unusual conditions (or variations). In everyday life, acclerative disruptions are fairly common, for instance when driving, flying, or boarding an aircraft or spacecraft.

The human body may unintentionally experience external accelerations in such circumstances. Such entire body accelerations have an impact on the subject's blood flow through the arteries [13], [14]. Although the human body is adaptable, long-term exposure to these acclerative disturbances can cause health issues like headache, abdominal pain, eyesight loss, and elevated heart rate. A mathematical model of blood flow in a single artery subject to pulsatile pressure gradient and body acceleration was presented by Sud and Sekhon [13] in 1985. A suspension model blood flow through an inclined tube with an axialy non-symmetric stenosis has been provided by Chakraborty et al. [4]. A theoretical model of pulsatile blood flow in a stenosed artery under the influence of periodic body accleration, with blood acting as a Casson fluid, was provided by Nagarani and Sarojamma [15]. By assuming a velocity slip condition at the constricted wall, Biswas and Chakraborty [16] constructed mathematical models for blood flow in stenosed arterial segments. So, it appears that taking a velocity slip at the stenosed vessel wall into account in blood flow modelling will be rather logical.

A 2-layered model of Bingham plastic flow through an asymmetrically constricted vessel with velocity slip at the interface has been attempted to investigate the effects of slip (at the asymmetric stenosis) and the influence of body acceleration on the flow variables (wall shear stress, velocity, flow rate, pressure gradient, and apparent viscosity). It is assumed that the flow is steady and laminar.

2. Mathematical Formulation

Blood flow through a constricted artery with an axially non-symmetrical but radially symmetrical stenosis is taken into consideration. The artery is assumed to be incompressible in the axial (Z) direction. The arterial constriction happens in the artery's lumen and is characterised by gradual alterations. In this inquiry, the stenosis's morphology is regarded as asymmetrical. In order to ignore the entrance and exit special wall effects, it is assumed that the artery length is sufficiently large compared to its radius. The centre of the sculpture is made up of a suspension of red blood cells. Two plasma layers—a central plasma layer and a peripheral plasma layer—are present in the outermost layer (as shown in Fig. 1). The rheology of blood in the core region has been categorised as a Newtonian fluid with varying viscosities and a non-Newtonian fluid that follows the Bingham fluid model, respectively.

Mathematically, the geometry of the stenosis that develops in the artery wall asymmetrically is modelled as [17]:

For PPL:

$$\frac{\overline{R}(\overline{z})}{\overline{R}_0} = 1 - \overline{G}\left[\overline{L_0^{m-1}}(z-d) - \left(\overline{z}-\overline{d}\right)^m\right],\ \overline{d} \le z \le \overline{d} + \overline{L_0} \tag{1}$$

$$= 1, \text{otherwise}$$

For the core region:

$$\frac{\overline{R_1}(\overline{z})}{\overline{R}_0} = \alpha - \overline{G_1}\left[\overline{L_0^{m-1}}(z-d) - \left(\overline{z}-\overline{d}\right)^m\right],\ \overline{d} \le z \le \overline{d} + \overline{L_0} \tag{2}$$

$$= \alpha, \text{otherwise}$$

where R(z) is the radius of the tube with stenosis, Ro is the constant radius of the tube, $R_1(z)$ is the radius of the artery in the core region such that $\alpha = (R_1(z))/R_0$, L_0 is the length of the stenosis, L is the

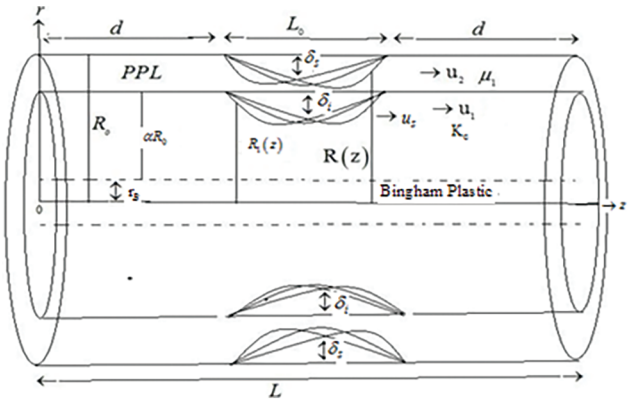

Fig. 1. The flow geometry of an axially symmetric arterial stenosis.

length of the tube, d is the stenosis location, δ_s and δ_i are the maximum height of the stenosis in the PPL and the core region respectively at $z = d + (L_0/2)$ such that the ratio of the stenotic height to the radius of the artery is very much less than unity i.e., $(\delta/R_0) << 1$ $G = (\partial s/(R_0 L_0^m))((m^{(m/m-1)})/(m-1))$, $G_1 = (\partial i/(R_0 L_0^m))((m^{(m/m-1)})/(m-1))$ where $m \geq 2$ is a parameter determining the shape of the stenosis. It is of interest to note that an increase in the value of m leads to the change of stenosis shape. When m = 2, the geometry of the stenosis becomes symmetrical at $z = d + (L_0/2)$ and $\alpha = \delta_i/\delta_s$.

2.1. Governing Equations and Boundary Conditions

It has been stated that for a low Reynolds number flow in a narrow tube with minor stenosis, the radial velocity is negligibly tiny and can be overlooked. The blood flow in the axial and radial directions is governed by momentum equations developed by Shankar and Ismail [18] as:

$$\overline{\rho}_B \frac{\partial \overline{u}_B}{\partial \overline{t}} = -\frac{\partial \overline{p}}{\partial \overline{z}} - \frac{1}{\overline{r}} \frac{\partial}{\partial \overline{r}} (\overline{r}\overline{\tau}_B) + \overline{F(t)},\ 0 \leq \overline{r} \leq \overline{R}_1(\overline{z}) \tag{3}$$

$$\overline{\rho}_N \frac{\partial \overline{u}_N}{\partial \overline{t}} = -\frac{\partial \overline{p}}{\partial \overline{z}} - \frac{1}{\overline{r}} \frac{\partial}{\partial \overline{r}} (\overline{r}\overline{\tau}_N) + \overline{F(t)}, \overline{R}_1(z) \leq \overline{r} \leq \overline{R}(\overline{z}) \tag{4}$$

In the core and peripheral regions respectively where $\overline{u}_B$ and $\overline{u}_N$ are the fluid velocities in the core region and peripheral region respectively; $\overline{\tau}_H, \overline{\tau}_N$ are the shear stresses for Bingham fluid and Newtonian fluid respectively; $\overline{\rho}_H, \overline{\rho}_N$ are the densities for Pulsatile fluid and Newtonian fluid; $\overline{p}$ the pressure and $\overline{F(t)}$ is the body acceleration.

The constitutive equations of Bingham fluid and Newtonian fluid are respectively given by:

$$\overline{\tau}_H = \overline{\tau}_y - \overline{\mu}_H \frac{\partial \overline{u}_H}{\partial \overline{r}}, if\ \overline{\tau}_H \geq \overline{\tau}_y, \overline{R}_H \leq \overline{r} \leq \overline{R}_1(\overline{z})$$

$$\frac{\partial \overline{u}_H}{\partial \overline{r}} = 0, \overline{\tau}_H \leq \overline{\tau}_y, 0 \leq \overline{r} \leq \overline{R}_H \tag{5}$$

$$\text{And } \overline{\tau}_N = -\overline{\mu}_N \frac{\partial \overline{u}_N}{\partial \overline{r}} \text{ if } \overline{R}_1(\overline{z}) \leq \overline{r} \leq \overline{R}(\overline{z}) \tag{6}$$

where $\overline{R}_p$ is radius of the plug core region. The periodic body acceleration in the axial direction is given by:

$$\overline{F}(\overline{t}) = A_0 \cos(\overline{\omega}_B t + \phi) \tag{7}$$

where A_0 is its amplitude, $\overline{\omega}_B = 2\pi \overline{f}_p$, $\overline{f}_p$ is its frequency in Hz, ϕ is the lead of $\overline{F}(\overline{t})$ w.r.t the heart action. The frequency of body acceleration $\overline{f}_p$ is assumed to be small so that wave effect can be neglected.

The pressure gradient at any $\overline{z}$ and $\overline{t}$ may be represented as follows:

$$-\frac{\partial \overline{p}}{\partial \overline{z}}(\overline{z}, \overline{t}) = A_0 + A_1 \cos(\overline{\omega}_p \overline{t}) \tag{8}$$

where A_0 is the steady component of the pressure gradient, A_1 is amplitude of the fluctuating component and $\overline{\omega}_B = 2\pi \overline{f}_p$, where $\overline{f}_p$ is the pulse frequency. Both A_0 and A_1 are functions of $\overline{z}$.

We introduce the non-dimensional variables:

$$z = \frac{\overline{z}}{\overline{R}_0},\ R(z) = \frac{\overline{R}(\overline{z})}{\overline{R}_0},\ R_1(z) = \frac{\overline{R}_1(\overline{z})}{\overline{R}_0},\ r = \frac{\overline{r}}{\overline{R}_0},$$

$$t = \overline{t}\overline{\omega}_p,\ \omega = \frac{\overline{\omega}_B}{\overline{\omega}_p},\ \delta_p = \frac{\overline{\delta}_p}{\overline{R}_0},\ \delta_B = \frac{\overline{\delta}_B}{\overline{R}_0},\ u_B = \frac{\overline{u}_B}{A_0 \overline{R}_0^2 / 4\overline{\mu}_B}$$

$$u_N = \frac{\overline{u}_N}{A_0 \overline{R}_0^2 / 4\overline{\mu}_N}, \tau_B = \frac{\overline{\tau}_B}{\overline{A}_0 \overline{R}_0}$$

$$\tau_N = \frac{\overline{\tau}_N}{\overline{A}_0 \overline{R}_0/2}, e = \frac{A_1}{A_0}, B = a_0/A_0, \theta = \frac{\overline{\tau}_y}{\overline{A}_0 \overline{R}_0/2}, \alpha_B^2 = \frac{\overline{R}_0^2 \overline{\omega}_p \overline{\rho}_B}{\overline{\mu}_c}, \alpha_N^2 = \frac{\overline{R}_0^2 \overline{\omega}_p \overline{\rho}_N}{\overline{\mu}_N}, \tag{9}$$

where α_B and α_N are the pulsatile Reynolds number for Bingham plastic fluid and Newtonian fluid respectively.

Using non-dimensional variables, (1) and (2) become:

Flow geometry for PPL:

$$\frac{R(z)}{R_0} = 1 - G\left[L_0^{m-1}(z-d) - (z-d)^m\right], d \leq z \leq d + L_0$$

$$= 1, \text{ otherwise} \tag{10}$$

For the core region:

$$\frac{R_1(z)}{R_0} = \alpha - G_1\left[L_0^{m-1}(z-d) - (z-d)^m\right], d \le z \le d + L_0$$
$$= \alpha, \text{ otherwise} \tag{11}$$

3. Boundary Conditions

The non-dimensional form's of boundary conditions are provided by:

$$\tau_B \text{ is finite at r} = 0 \tag{12}$$

$$u_N = \text{u}_s \text{ at } r = \text{R(z)} \tag{13}$$

$$\tau_B = \tau_N, u_B = u_N \text{ at } r = R_1(z), \tag{14}$$

The non-dimensional form of the governing equations of motion provided by (3) and (4) is:

$$\alpha_B^2 \frac{\partial u_B}{\partial t} = 4(1 + e\cos\theta) + 4B\cos(\omega t + \psi) - \frac{2}{r}\frac{\partial}{\partial r}(r\tau_B), 0 \le r \le R_1(z), \tag{15}$$

$$\alpha_N^2 \frac{\partial u_N}{\partial t} = 4(1 + e\cos\theta) + 4B\cos(\omega t + \psi) - \frac{2}{r}\frac{\partial}{\partial r}(r\tau_N), R(z) \le r \le R_1(z), \tag{16}$$

Equations (5) and (6) are reduced by using non-dimensional variables as follows:

$$\tau_B = \theta - \frac{1}{2}\frac{\partial u_B}{\partial r}, \text{if } \tau_B \ge \theta, R_p \le r \le R_1(z), \tag{17}$$

$$\frac{\partial u_B}{\partial r} = 0, if\, \tau_B \le \theta, 0 \le r \le R_p \tag{18}$$

$$\frac{\partial u_N}{\partial r} = 0, \text{if } R_1(z) \le r \le R(z) \tag{19}$$

The dimensionless volumetric flow rate is given by:

$$Q(z,t) = 4\int_0^{R(z)} u_B(r,z,t)\, rdr \tag{20}$$

where $Q(z,t) = (\overline{Q}(\overline{z},\overline{t}))/(\pi(\overline{R}_0)^4 A_0/8\overline{\mu}_B)$, $\overline{Q}(\overline{z},\overline{t})$ is the volumetric flow rate.

The effective viscosity $\overline{\mu}_a$ defined as:

$$\overline{\mu}_a = \pi\left(-\frac{\partial\overline{p}}{\partial\overline{z}}\right)(\overline{R}(\overline{z}))^4/\overline{Q}(\overline{z},\overline{t}), \tag{21}$$

Can be expressed in dimensionless form as:

$$\mu_a = (R(z))^4(1 + e\cos t)/Q(z,t) \tag{22}$$

4. Method of Solution

It is important to expand (15), (16), and (17)–(19) in perturbation series about α_B^2 and α_N^2 since α_B^2, α_N^2 are time dependent, we expand u_B, R_p, and u_N as follows:

$$u_B(z,t) = u_{oB}(z,t) + u_{1B}(z,t) + \ldots \tag{23}$$

$$R_B(z,t) = R_{0B}(z,t) + R_{1B}(z,t) + \ldots \tag{24}$$

$$u_B(z,r,t) = u_{0N}(z,t) + \alpha_N^2 u_{1N}(z,r,t) + \ldots$$

Equating powers of α_B^2, the resulting equations of the core region can be obtained as:

$$\frac{\partial}{\partial r}\left(r\tau_{0B}\right)=2f\left(t\right)r,\frac{\partial u_{0B}}{\partial t}=-\frac{2}{\partial r}\left(r\tau_{1B}\right),-\frac{\partial u_{1B}}{\partial t}=2\tau_{1B} \tag{25}$$

Similarly using the perturbation series expansions in (16) and (19) and equating powers of α_N^2, the resulting equations of the peripheral region can be obtained as:

$$\frac{\partial}{\partial r}\left(r\tau_{0N}\right)=2f\left(t\right)r,\frac{\partial u_{0N}}{\partial t}=-\frac{2}{\partial r}\left(r\tau_{1N}\right),-\frac{\partial u_{1N}}{\partial t}=2\tau_{1N} \tag{26}$$

Using the perturbation series expansions in (12)–(14) and equating constant terms and terms containing α_B^2 and α_N^2, we get:

$$\tau_{0B}\text{ and }\tau_{1B}\text{ are finite at r = 0,}$$

$$\begin{aligned}&\tau_{0B}=\tau_{0N},\tau_{1B}=\tau_{1N},u_{0B}=u_{0N},u_{1B}=u_{1N},\text{at }r=R_1\left(z\right),\\&u_{0N}=u_s,u_{1N}=0\text{ at }r=R\left(z\right)\end{aligned} \tag{27}$$

On solving (25) and (26) for unknowns $u_{0p}, u_{1p}, u_{0B}, u_{1B}, u_{0N}, u_{1N}, \tau_{0B}, \tau_{1B}, \tau_{0N}, \tau_{1N}$ using (27), we can obtain:

$$\tau_{0B}=f\left(t\right)r,\tau_{0N}=f\left(t\right)r, \tag{28}$$

$$u_{0N}=u_s+f\left(t\right)\left(\left(R\left(z\right)\right)^2-r^2\right), \tag{29}$$

$$u_{0B}=u_s+f\left(t\right)\left(\left(R\left(z\right)\right)^2-r^2\right)-2kf\left(t\right)\left(R_1\left(z\right)-r\right), \tag{30}$$

$$u_{0p}=u_s+f\left(t\right)\left(\left(R\left(z\right)\right)^2-{R_{0p}}^2\right)-2kf\left(t\right)\left(R_1\left(z\right)-R_{0p}\right), \tag{31}$$

$$\tau_{1B}=-\frac{f'\left(t\right)}{24}\left[6\left(R\left(z\right)\right)^2r-3r^3-4k\left(3R_1\left(z\right)r-2r^2\right)\right], \tag{32}$$

$$\tau_{1N}=-\frac{f'\left(t\right)}{24}\left[6\left(R\left(z\right)\right)^2r-3r^3-4k\frac{\left(R_1\left(z\right)\right)^3}{r}\right], \tag{33}$$

$$u_{1N}=\frac{f'\left(t\right)}{48}\left[12\left(R\left(z\right)\right)^2r^2-3r^4-9\left(R\left(z\right)\right)^4-16k\left(R\left(z\right)\right)^3\ln\left(\frac{r}{R\left(z\right)}\right)\right], \tag{34}$$

$$\begin{aligned}u_{1c}=&\frac{f'\left(t\right)}{48}\left[12\left(R\left(z\right)\right)^2r^2-3r^4-9\left(R\left(z\right)\right)^4\right.\\&\left.-4k\left\{6R_1(z)r^2-\frac{8}{3}r^3-\frac{10}{3}\left(R_1(z)\right)^3+\left(R_1(z)\right)^3\ln\left(\frac{R_1(z)}{R(z)}\right)\right\}\right],\end{aligned} \tag{35}$$

$$u_{1p}=\frac{f'\left(t\right)}{48}\left[\begin{aligned}&12\left(R\left(z\right)\right)^2{R_{0p}}^2-3{R_{0p}}^4-9\left(R\left(z\right)\right)^4\\&-4k\left\{6R_1\left(z\right)r^2-\frac{8}{3}r^3-\frac{10}{3}\left(R_1\left(z\right)\right)^3+\left(R_1\left(z\right)\right)^3\ln\left(\frac{R_1\left(z\right)}{R\left(z\right)}\right)\right\}\end{aligned}\right] \tag{36}$$

where $k=\theta/f\left(t\right)$.

Neglecting the terms of $o\left(\alpha_B^2\right)$ and higher powers of α_B in (24), the first approximation plug core radius R_{0p} can be obtained as:

$$R_{0p}=\frac{\theta}{f\left(t\right)}=k \tag{37}$$

Using (29), (30), (34) and (35) the expressions for axial velocities in the core and peripheral regions are obtained as:

$$\begin{aligned}u_N=&u_s+f\left(t\right)+\left(R\left(z\right)\right)^2-r^2)\\&+\frac{\alpha_N^2f'\left(t\right)}{48}\left[12\left(R\left(z\right)\right)^2r^2-3r^2-9\left(R\left(z\right)\right)^4-16k\left(R_1\left(z\right)\right)^3\ln\left(\frac{r}{R\left(z\right)}\right)\right]\end{aligned} \tag{38}$$

$$u_B = u_s + f(t)\left((R(z))^2 - r^2\right) - 2kf(t)(R_1(z) - r) + \frac{\alpha_N^2 f'(t)}{48}\left[12(R(z))^2 r^2 - 3r^4 - 9(R(z))^4 - 4k\left(6R_1(z)r^2 - \frac{8}{3}r^3 - \frac{10}{3}(R_1(z))^3 + (R_1(z))^3 \ln\left(\frac{R_1(z)}{R(z)}\right)\right)\right] \tag{39}$$

The expression for plug-core velocity can also be easily calculated using (23), (31) and (36) in a similar manner.

The expression for wall shear stress τ_w can be obtained by:

$$\tau_w = \left(\tau_{0N} + \alpha_N^2 \tau_{1N}\right)_{r=R(z)}, \tag{40}$$

$$= f(t)R(z) - \frac{\alpha_N^2 f'(t)}{48}\left[3(R(z))^3 - 4k\frac{(R_1(z))^3}{R(z)}\right] \tag{41}$$

From (20), (38) and (39) the volumetric flow rate is given by:

$$= 2u_s R^2 + f(t)\left[R^4 - R_{0p}^4 - \frac{4k^2}{3}\left(R_1^3 - R_{0p}^3\right)\right] + \frac{f'(f)\alpha_B^2}{24}\left[6R^2R_{0p}^4 - 2R_{0p}^6 - R_1^6 + 6R^2R_1^4 - 9R^4R_1^2 - 4k\left\{3R_1R_{0p}^4 - \frac{8}{5}R_{0p}^5 - \frac{7}{5}R_1^5 + R_1^5\ln\left(\frac{R_1}{R}\right)\right\}\right] + \frac{f'(f)\alpha_N^2}{24}\left[9R^4R_1^2 - 6R^2R_1^4 - 4R^6 + R_1^6 + 8k\left\{2R_1^5\ln\left(\frac{R_1}{R}\right) + R^2R_1^3 - R_1^5\right\}\right] \tag{42}$$

where R = R(z), $R_1 = R_1(z)$. The expression for effective viscosity μ_a can be obtained from (22) and (42).

The second approximation plug core radius R_{1p} can be obtained by neglecting terms of $o\left(\alpha_B^4\right)$ and higher powers of α_B in (26) as:

$$R_{1p} = -\frac{\tau_{1B}(R_{0p})}{f(t)} = -\frac{f'(f)k^2}{24}\left(6R^2 - 5k - 12R_1\right) \tag{43}$$

From (24), (37) and (43), the expression for plug core radius can be obtained as:

$$R_p = k - \frac{f'(t)k^4}{24}\left(6R^2 - 5k^2 - 12R_1\right) \tag{44}$$

The flow system represented by (38)–(42) reduces to a one-layered Newtonian flow system with body accleration as the lack of yield stress, i.e., τ_0 and a peripheral plasma layer (i.e., $(\alpha = 1, R(z) = R_1(z))$).

$$u = u_s + f(t)\left((R(z))^2 - r^2\right) + \frac{\alpha^2}{16}f'(f)\left(4(R(z))^2 r^2 - 3(R(z))^4 - r^4\right), \tag{45}$$

$$Q = (R(z))^2\left\{2u_s + f(t)(R(z))^2 - \frac{\alpha^2}{6}f'(t)(R(z))^4\right\}, \tag{46}$$

$$\tau_w = f(t)R(z) - \frac{\alpha^2}{8}f'(t)(R(z))^3, \tag{47}$$

$$\mu_B = (R(z))^2(1 + e\cos t)\left\{2u_s + f(t)(R(z))^2 - \frac{\alpha^2}{6}f'(t)(R(z))^4\right\}^{-1} \tag{48}$$

5. Results and Discussions

In order to study the combined effects of body acceleration, stenosis, and velocity slip on the flow variables—axial velocity, flow rate, shear stress, and effective viscosity of blood—flowing in an artery with a modest constriction, the current model has been created. Using a perturbation analysis with very small Womersley frequency parameters ($\alpha_B = \alpha_N = 0.5 < 1$), the equations governing the aforementioned flow are integrated. The lead angle ϕ is taken to be 0.2 and the height of the stenosis δ_p in the peripheral region is taken to be in the range of 0–0.5. It is assumed that the body acceleration parameter B is in the range of 0–2, and that the pressure gradient parameter e is in the range of 0–5. The central core radius to the normal radius of the artery is assumed to be 0.8, the yield stress is assumed to be 0 and 0.1, and the value of z is assumed to be between -4 and 4. The axial velocity slip is estimated to be between 0 and 0.1.

Figs. 2 and 3 illustrates the relationship between axial velocity and radial distance using (38) and (39) for constant values of peripheral stenosis height δ_p, pressure gradient e, time duration t, and for various values of slip velocity us and body acceleration parameter B.

It is noted from the picture that axial velocity is maximum at r = 0, where from it gradually drops with the rise in radius of the artery r and attains a minimum value at the stenotic wall (r = R(z)) for any value of body acceleration parameter B. Yet, using slip at the wall causes the axial velocity to increase. Axial velocity is further enhanced by an increase in body acceleration. Fig. 5 shows the variation in volumetric flow rate with respect to the pressure gradient parameter e for constant values of peripheral stenosis height δ_p, time t, and for various values of slip velocity u_s, yield stress, and body acceleration parameter B. For any value of B and, it has been found that flow rate gradually rises as the pressure gradient parameter e increases. Yet, the flow rate is greater in the absence of yield stress (τ_0) than it is when yield stress is present. Further observation reveals that using body acceleration enhances flow

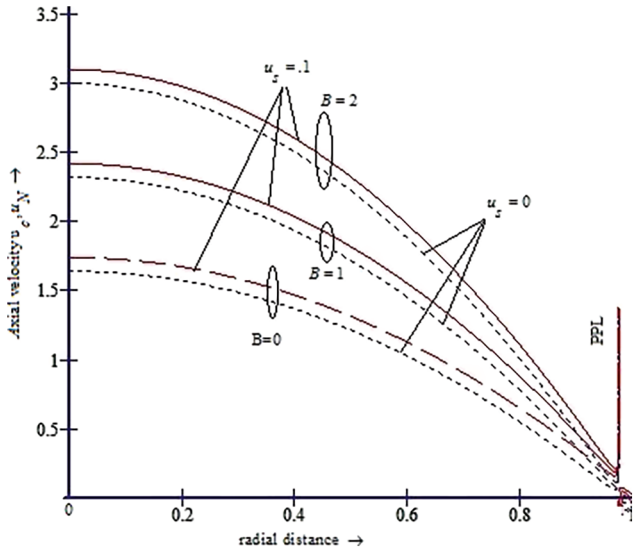

Fig. 2. Variation of axial velocity with radial distance for t = 45°, e = 1, $\alpha = 0.8$, B = 0, 1, 2 and different values of z and u_s.

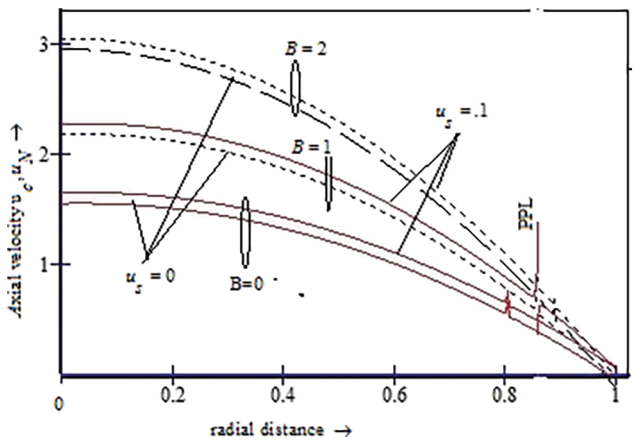

Fig. 3. Variation of axial velocity with radial distance for t = 45°, e = 1, $\alpha = 0.8$, B = 0, 1, 2 and different values of z and u_s.

rate. Fig. 6, which show the variation of wall shear stress with axial distance z and time t, respectively. As seen in the figures, wall shear stress ζ_w increases from its approached magnitude (i.e., at z = -4) in the upstream of the throat with the axial distance and reaches its maximum at the throat of the stenosis. From there, it decreases in the downstream and attains a lower magnitude at the end of the constriction profile (i.e., at z = 4). The magnitude of wall shear stress τ_w in a uniform tube ($\delta_p = 0$) is less than that of an artery with stenosis ($\delta_p > 0$) increases noticeably for any value of the body acceleration parameter B with the height of the peripheral stenosis δ_p. For any value of the body acceleration parameter B, it is also seen that the wall shear stress τ_w, progressively declines over time until it achieves its minimum at time t = 180°, after which it gradually increases over time until it reaches its peak magnitude at time t = 360°. Fig. 4 shows visual representations of the variations in effective viscosity (μ_a) with axial distance (z) and peripheral stenosis height (δ_p), respectively. Effective viscosity rises with axial distance z from the beginning of a stenosis (i.e., at z = -4) to the throat (i.e., at z = 0), where it reaches its greatest value, before gradually falling to its original value at the stenosis' termination (i.e., at z = 4). Additionally, the findings show that for both no-slip and slip at wall scenarios, effective viscosity μ_a rises with the height of peripheral stenosis. Yet, for any value of the body acceleration parameter B, using an axial slip velocity at the wall reduces the effective viscosity in both the presence and absence of yield stress. Given fixed values of B and u_s, effective viscosity increases with yield stress, body acceleration decreases wall shear stress in both uniform ($\delta_p = 0$) and stenosed ($\delta_p > 0$) arteries.

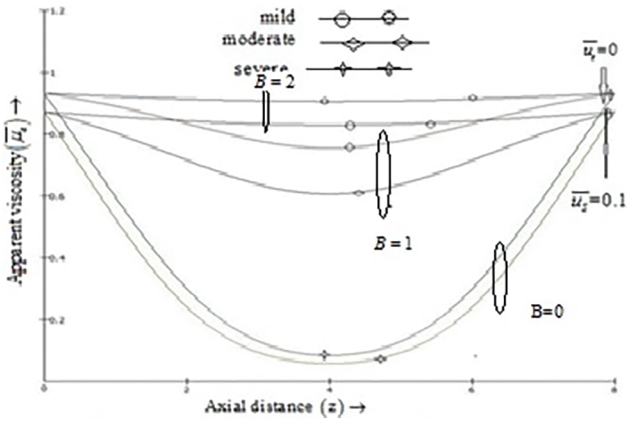

Fig. 4. Variation of apparent viscosity with axial distance for B = 1, $\delta_p = 0.2$, t = 45°, z = 0, $\beta = 0.8$.

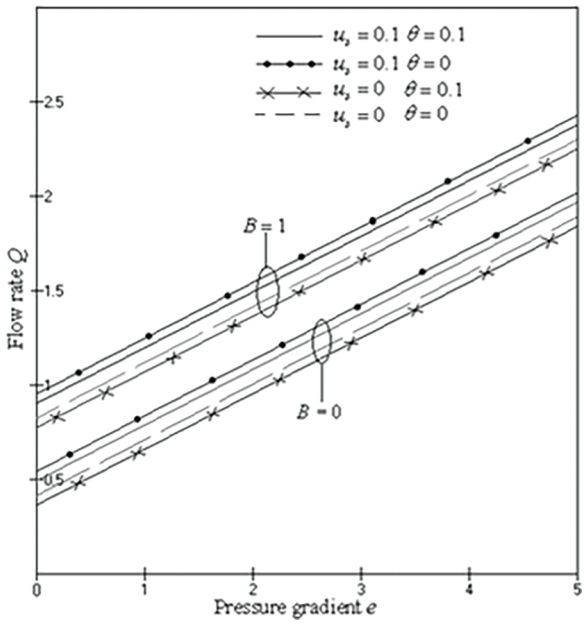

Fig. 5. Variation of flow rate with pressure gradient for B = 1, $\delta p = 0.2$, t = 45°, z = 0, b = 0.8.

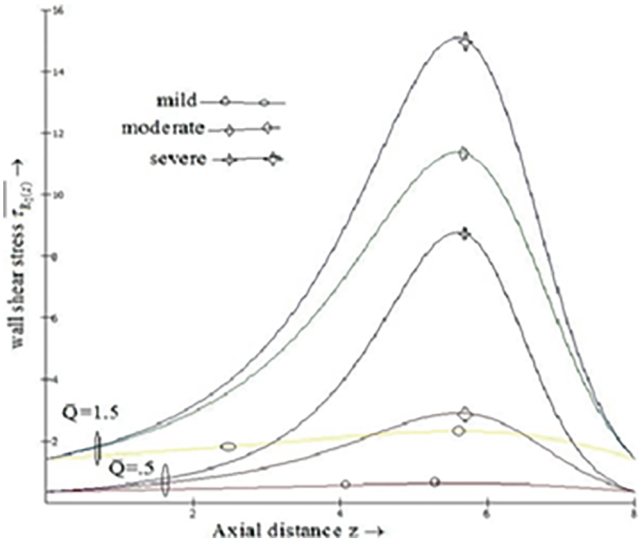

Fig. 6. Variation of wall shear stress against axial distance with time for $g = 0.1$, $b = 0.8$, $z = 0$.

6. Conclusions

The two-layered pulsatile blood flow through an artery (Fig. 1) embedded with an axi-symmetric moderate stenosis is the subject of the current analysis, and an axial velocity slip is used at the constricted wall. Blood is modelled as Bingham Plastic in the core region and is believed to behave as a Newtonian fluid in the periphery plasma layer. A perturbation method is used to integrate the motion equations that control the flow. It is possible to obtain analytical formulas for flow variables, and their variations with various flow parameters are graphically displayed. As anticipated, it is seen that wall slip causes a drop in effective viscosity while increasing axial velocity and flow rate. Also wall shear stress and effective viscosity decrease but velocity and flow rate increase with the body acceleration parameter B. Effective viscosity μ_e increases as μ_p increases. However, μ_B is lowered for both the uniform tube ($\delta_s = 0$) and stenosed artery ($\delta_p > 0$) as a result of wall slip. Since this study takes care of pulsatibility of the flow and also it incorporates the characteristics of non-Newtonian nature of blood, so it is well mentioned that the present model could play a pivotal role to study the flow of blood. From the analysis, it may also be concluded that with slip, the damages to the vessel wall could be lowered. This type of decrease in wall shear stress and effective viscosity may be used to improve the health and performance of diseased arterial systems. So, one may search for medications or equipment that causes slip and use it to treat peripheral arterial illnesses. The permeability of the blood vessels could be taken into account to further enhance the model.

References

[1] Guyton AC. *Text Book of Medical Physiology*. Philadelphia: W.B. Saunders; 1970.
[2] Boyd W. *Text Book of Pathology: Structure and Functions in Diseases*. Philadelphia: Lea and Febigar; 1960.
[3] Biswas, D. *Blood Flow Models: A Comperative Study*. Mittal Publications, New Delhi.
[4] Ponalgusamy R. Blood flow through an artery with mild stenosis-a two-layered model, different shapes of stenosis and slip velocity at the wall. *J Appl Sci*. 2007;7:1071–77.
[5] Biswas D, Chakraborty US. Pulsatile blood flow in a constricted artery with body acceleration. *Appl Math*. 2009;4:329–42.
[6] Bugliarello G, Sevilla J. Velocity distribution and other characteristics of steady and pulsatile blood flow in fine glass tubes. *Biorheology*. 1970;17:85–107.
[7] Cockelet GR. The rheology of human blood. In *Biomechanics*. New Jersey: Prentice Hall, Englewood Cliffs; 1972.
[8] Fung YC. *Biomechanics: Mechanical Properties of Living Tissues*. New York Inc: Springer-Verlag; 1981.
[9] Kapur JN, Bhatt BS, Sacheti NC. *Non-Newtonian Fluid Flows (A survey monograph)*. Meerut, India: Pragati Prakashan; 1982.
[10] Schlichting H. *Boundary Layer Theory*. New York: Mc Graw-Hill Book Company; 1968.
[11] Chaturani P, Samy SP. A two-layered model for blood flow through Stenosed Arteries. *Proc. 11th Nat. Conference on Fluid Mechanics and Fluid Power, I.C.F. 16.9*, 1982.
[12] Guyton AC and Hall JE. *Text Book of Medical Physiology*. Elsevier; 2006.
[13] Sud VK, Sekhon GS. Arterial flow under periodic body acceleration. *Bull. Math. Biol*. 1985;47(1):35–52.
[14] Sud VK, Sekhon GS. Flow through a stenosed Artery subject to periodic body acceleration. *Med. Biol. Eng. & Comput*. 1987;25:638–44.
[15] Nagarani P, Sarojamma G. Effect of body acceleration on pulsatile flow of Casson fluid through a mild stenosed artery. *Korea Aust Rheol J*. 2008;20(4):189–96.
[16] Biswas D, Chakraborty US. A brief review on blood flow modeling in arteries. *Assam Univ J Sci Technol*. 2010;6:10–5.

[17] Ponalagusamy R. Blood flow through stenosed tube. Ph.D Thesis, IIt, Bombay, India; 1986.
[18] Sankar DS, Ismail AMd. Two-fluid mathematical models for blood flow in stenosed artery: a comparative study. *Bound Value Probl*. 2009;2009:1–15.